Molecular Imaging Using High-Order Harmonic Generation and Above-Threshold Ionization

Elmar V. van der Zwan[1,2] and Manfred Lein[1]

[1]*Institut für Theoretische Physik and Centre for Quantum Engineering and Space-Time Research (QUEST), Leibniz Universität Hannover, Appelstraße 2, D-30167 Hannover, Germany*

[2]*Institut für Physik, Universität Kassel, Heinrich-Plett-Straße 40, D-31432 Kassel, Germany*

(Received 24 July 2011; published 25 January 2012)

Accurate molecular imaging via high-order harmonic generation relies on comparing harmonic emission from a laser-irradiated molecule and an adequate reference system. However, an ideal reference atom with the same ionization properties as the molecule is not always available. We show that for suitably designed, very short laser pulses, a one-to-one mapping from high-order harmonic frequencies to electron momenta in above-threshold ionization exists. Comparing molecular and atomic momentum distributions then provides the electron recollision amplitude in the molecule for enhanced molecular imaging. The method retrieves the molecular recombination transition moments highly accurately, even with suboptimal reference atoms.

DOI: 10.1103/PhysRevLett.108.043004 PACS numbers: 33.80.Rv, 42.65.Ky

When atoms or molecules are irradiated by a strong laser field, high-order harmonic generation (HHG) takes place and high-frequency photons are emitted [1]. The interest in HHG from molecules is growing since observing the radiation is a tool to investigate the structure of molecules [2–11]. The sensitivity of the emission spectra to the target structure can be understood within the three-step model, which provides a semiclassical interpretation of HHG in terms of (i) ionization, (ii) free propagation of the electron in the laser field and return to the parent ion, and (iii) recombination [12]. In good approximation, the HHG intensity is proportional to the modulus squared of the recombination transition dipole moment, or equivalently to the recombination cross section [3,13–15]. When the electron continuum states are additionally approximated as plane waves, one can obtain molecular orbitals via a tomographic retrieval based on the Fourier transform of the HHG amplitudes measured from aligned molecules [3,9]. Laser-based imaging is of high interest because it can reveal structural changes of matter on the few-fs and sub-fs time scales. The HHG-based molecular-imaging methods rely on the comparison of the harmonic emission to that of a reference system with known electronic structure, typically a reference atom. Assuming that the molecule and the reference atom have the same properties concerning ionization and electron propagation, the recombination cross section of the molecule can be isolated. Clearly, no reference atom with exactly the same ionization properties as the molecule exists. Therefore, a systematic method to correct for these deviations is highly desirable.

Since the probability for recombination of a returning electron is very small, it is likely that the system remains ionized, and the electron can be detected as an above-threshold ionization (ATI) electron. ATI momentum distributions have also been used for molecular imaging [14,16,17]. It appears plausible to combine HHG and ATI to improve laser-based molecular imaging. For reasons outlined in the following, however, no concrete method has been proposed up to now apart from using the orientation dependence of the total ionization probability [3] which accounts for the suppression of ionization and HHG due to nodal planes.

Usually, multicycle laser pulses have been used to drive HHG and ATI. This means that many different electron trajectories can potentially contribute to the same harmonic frequency or to the same electron momentum. In the case of HHG, the same frequency is generated twice per optical half cycle, namely, by the well-known short and long trajectories [18]. In the case of ATI, the interference of contributions from two ionization times has been termed attosecond double-slit interference [19].

Initially it was thought there would be a direct correspondence between the HHG and ATI spectra, see [20] and references therein, and attempts were made to express the harmonic yield as a sum over ATI channels plus recombination [21,22]. However, no direct link between the intensities of individual HHG and ATI peaks could be drawn as in general it is impossible to disentangle the contributions from different trajectories. Two trajectories producing the same harmonic frequency will generally lead to different ATI energies. In the present work we show that for extremely short pulses with suitable carrier-envelope phase this link is possible because only a very limited number of trajectories contribute. We present strong one-to-one links from HHG frequencies to ATI momenta, based on shared birth times of the HHG and ATI trajectories. We show how to use the relation between HHG and ATI to improve molecular-imaging methods such as orbital tomography in order to retrieve molecular properties with high accuracy.

If there is only one trajectory contributing to each ATI momentum and HHG frequency, and if both trajectories

are born at the same time, the ionization steps are identical and there is a one-to-one mapping from HHG frequency ω to ATI momentum $p^{(A)}(\omega)$. We assume here that the ATI electron is emitted along the laser polarization axis, and we neglect rescattering ATI. Then, the HHG intensity $S(\omega) = |\boldsymbol{\alpha}(\omega)|^2$ and ATI momentum distribution $A(p) = |M(p)|^2$ are related by (atomic units are used throughout) [12,13,23]

$$\boldsymbol{\alpha}(\omega) = a(\omega)\mathbf{d}_r(\omega), \tag{1a}$$

$$A(p^{(A)}(\omega)) = C(\omega)|a(\omega)|^2. \tag{1b}$$

Here, the complex amplitude $\boldsymbol{\alpha}(\omega)$ is the Fourier transformed dipole acceleration and the recollision amplitude $a(\omega)$ describes the continuum wave packet for HHG. The recombination transition dipole moment for the HHG process is $\mathbf{d}_r(\omega) = \langle\psi_{\mathbf{k}}|\hat{\mathbf{D}}|\psi_0\rangle$ with bound state ψ_0, continuum state $\psi_{\mathbf{k}}$, and dipole operator $\hat{\mathbf{D}}$. The factor $C(\omega)$ relates HHG and ATI and includes the effect of electron motion after the return time on the momentum distribution. Below, we confirm that $C(\omega)$ only depends on the laser field and is independent of the atom or molecule. This is in contrast to the quantity $a(\omega)$, which is also species dependent. Thus, if the momentum distributions $A(p)$ are known for two different systems, the ratio of their factors $|a(\omega)|$ can be obtained from Eq. (1b).

Before demonstrating the improved molecular-imaging scheme, we find suitable laser pulses for which the one-to-one mapping holds. To this end, we express the HHG and ATI yields using the strong-field approximation and expand around classical trajectories. For HHG we employ the Lewenstein model [18]. In this model, the saddle-point integration over momentum gives the saddle-point momentum $k_s(t,t') = -\int_{t'}^{t} A(t'')dt''/(t-t')$ with $A(t) = -\int_{-\infty}^{t} E(t'')dt''$ such that an electron born at time t' returns to its initial position at recombination time t for a linearly polarized laser field $E(t)$. In contrast to [13,24], we perform both remaining integrations over t' and t using the saddle-point method. The resulting spectrum is formed by trajectories with complex saddle-point times t_s' and t_s, starting with imaginary initial momentum $v_i = -i\mathrm{sgn}(E(t_0'))\sqrt{2I_p}$ and returning with momentum $v_r = \pm\sqrt{2(\omega - I_p)}$, where I_p is the ionization potential. The classical ionization and recombination times t_0', t_0 are defined by setting $v_i = 0$ instead of an imaginary velocity, while still requiring a classical trajectory from t_0' to t_0 including only the force due to the laser field. We employ a very short pulse such that all return momenta v_r have the same sign (chosen negative here) [25]. We write $|v_i| = \beta$ and expand the times t_s', t_s around t_0', t_0' to second order in the parameter β. We obtain $t_s = t_0 + \frac{1}{2}b_2\beta^2$ and $t_s' = t_0' + a_1\beta + \frac{1}{2}a_2\beta^2$ with

$$a_1 = i/|E(t_0')|, \tag{2a}$$

$$a_2 = f(t_0, t_0')/(E(t_0'))^2, \tag{2b}$$

$$b_2 = 1/[E(t_0')(v_r + \tau_0 E(t_0))], \tag{2c}$$

where $f(t_0, t_0') = \frac{E(t_0)}{v_r + \tau_0 E(t_0)} + \frac{E'(t_0')}{E(t_0')}$ and $\tau_0 = t_0 - t_0'$. Expanding the action $S(t,t') = \frac{1}{2}\int_{t'}^{t} dt''[k_s(t,t') + A(t'')]^2 + I_p(t-t')$ to fourth order, the resulting expression in a d-dimensional world is, denoting $\tau_s = t_s - t_s'$,

$$\boldsymbol{\alpha}(\omega) = i\omega^2\left(\frac{8}{I_p}\right)^{1/4}\mathbf{d}^*_{\mathrm{r,pw}}(v_r)\sum_{t_0,t_0'}\left[\frac{2\pi}{\epsilon + i\tau_s}\right]^{d/2} d_i(v_i, t_s')e^{-i(S(t_0,t_0')-\omega t_0)}e^{-((2I_p)^{3/2})/(3|E(t_0')|)}e^{(if(t_0,t_0')I_p^2)/(2(E(t_0'))^2)}$$

$$\times\sqrt{\frac{\pi}{f(t_0,t_0')i|v_i| + |E(t_0')|}}\sqrt{\frac{\pi i\tau_s/v_r}{v_r + \tau_s E(t_s)}}, \tag{3}$$

with the plane-wave recombination transition moment $\mathbf{d}_{\mathrm{r,pw}}$. The ionization plane-wave matrix element

$$d_i(k,t) = \frac{E(t)}{(2\pi)^{d/2}}\int \psi_0(\mathbf{r})xe^{-ikx}d^d\mathbf{r} \tag{4}$$

exhibits a pole at the saddle-point momentum for Coulombic potentials [26], but HHG can be modeled successfully using Gaussian bound states that do not exhibit the pole [18]. Since we do not use the model to calculate orientation dependences, we replace the integral in Eq. (4) by an arbitrary constant. This simplification does not affect the shape of the HHG spectra or the relative weights of different trajectories.

Similarly, we expand the ATI amplitude $M(p)$ as given by Milošević *et al.* [27–29] around classical birth times. For detailed derivations of Eqs. (2) and (3) and the analogous ATI expression, see [30]. The sum in Eq. (3) and its ATI equivalent is normally over several possible trajectories. Our objective is to design pulses such that only one term dominates each sum. We calculate the uniqueness of a trajectory in determining harmonic frequency ω by dividing the absolute value of the corresponding term in Eq. (3) by the sum over absolute values. For every harmonic trajectory we also calculate the uniqueness of the ATI trajectory born at the same time in determining its associated ATI momentum. The maximum attainable product of these two factors is the HHG-to-ATI link $Q(\omega)$. For the maximum possible value $Q = 1$, there is a perfect correspondence between a harmonic frequency and ATI momentum through their shared birth time. In Fig. 1(a) we

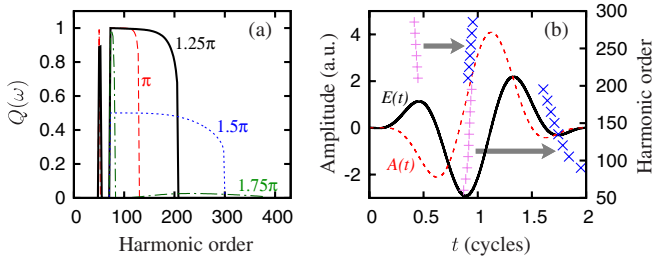

FIG. 1 (color online). (a) HHG-to-ATI link $Q(\omega)$ for two-cycle $\sin^2$ pulses with $\phi_{\mathrm{CEP}} = \pi$ (red dashed line), $\phi_{\mathrm{CEP}} = 1.25\pi$ (black solid line), $\phi_{\mathrm{CEP}} = 1.5\pi$ (blue dotted line), and $\phi_{\mathrm{CEP}} = 1.75\pi$ (green dot-dashed line); (b) laser field $E(t)$ ($\times 40$, black solid line) and $A(t)$ (red dashed line) for $\phi_{\mathrm{CEP}} = 1.25\pi$. Also indicated are the birth (violet plusses) and recombination (blue crosses) times of the trajectories dominating the HHG signal, plotted as harmonic order versus time.

show $Q(\omega)$ for different two-cycle $\sin^2$-laser pulses with intensity 2×10^{14} W/cm^2 and wavelength 2000 nm shining on a 1D system with the ionization potential set to $I_p = 30.2$ eV, which is very close to the vertical ionization potential 30 eV of real H_2^+ at the equilibrium distance. The results do not depend critically on I_p and they are nearly independent of the dimensionality d (not shown). The pulses are characterized by the carrier-envelope phase ϕ_{CEP}, i.e., the phase between the envelope and the carrier wave of the pulse. We only consider links with absolute ATI momenta above 1 a.u.

A two-cycle pulse with $\phi_{\mathrm{CEP}} = 1.25\pi$ gives a good link between HHG and ATI over a broad harmonic range starting from harmonic order 70. This matches the frequency range where molecule-specific interference signatures appear in H_2^+ and H_2 [2]. In Fig. 1(b) we plot the time-dependent electric field and vector potential of this pulse, and we indicate the birth and recombination times of the trajectories dominating the HHG signal. Because $|E(t)|$ is much higher during the birth time of harmonic orders $\sim$100–200 ($t \simeq 0.92T$) than around $t \simeq 1.35T$—the only other time where ATI electrons with the same final momentum are born—the link between HHG and ATI arises. Smartly selecting experimental phase-matching conditions might allow somewhat longer pulses to provide useful links between HHG and ATI. However, for slightly longer pulses the HHG frequencies are linked to very low ATI momenta. This may require that the link is calculated using modified classical trajectories to account for the Coulomb force in addition to the laser field.

We verify the link between HHG and ATI by numerical solution of the time-dependent Schrödinger equation (TDSE) for 1D H_2^+ with varying internuclear distance R. We use the softcore potential

$$V(x) = \frac{-Z}{\sqrt{\left(x - \frac{R}{2}\right)^2 + a^2}} - \frac{Z}{\sqrt{\left(x + \frac{R}{2}\right)^2 + a^2}}. \quad (5)$$

Here and below, the softness parameter a^2 is always adjusted such that $I_p = 30.2$ eV. The TDSE is solved on a grid using the split-operator method [31], and the bound states are found by imaginary-time propagation [32]. The grid length is 24 027 a.u. and it contains 143 360 grid points. After the end of the laser pulse, the wave function is propagated for two more cycles. The HHG spectrum is calculated from a windowed Fourier transform of the dipole acceleration and the ATI spectrum is obtained from the momentum-space representation of the wave function after removing the bound states by windowing out the inner 40 a.u. in position space. For the ground state with $Z = 0.731$ and three different internuclear distances, the HHG spectra and ATI momentum distributions are shown in Fig. 2 using the pulse of Fig. 1(b). Although the variation of R seems to have little effect on the overall spectra, the insets show that the details of HHG and ATI spectra are very sensitive to R, in particular, in the dominant spectral regions. HHG is suppressed near the ionization threshold at harmonic order 49 since the dominant trajectory for this laser pulse generates harmonics in the range from 55 to 215. To obtain the HHG recollision amplitude $a(\omega)$, we proceed similar to the quantitative rescattering theory [14,23]. We calculate the 1D transition moments $d_r = \langle \psi_k | x | \psi_0 \rangle$ with field-free scattering states ψ_k. We obtain numerically exact ψ_k by integrating the static Schrödinger equation using the Numerov method [33] on a grid with a total length of 4000 a.u. and 320 000 grid points. For an electron approaching from positive x with momentum $k < 0$, we set the wave function equal to a transmitted wave $\exp(ikx)$ at the two lowest grid points. After obtaining a numerical wave function $\varphi_k(x)$ by integrating upwards, the properly normalized wave function $\psi_k(x) = c\varphi_k(x)$ follows by requiring a superposition of incoming plane wave and reflected plane wave at the upper end $x_{\max}$ of the grid,

$$\psi_k(x) = e^{ikx} + re^{-ikx}, \quad (6)$$

where r is the reflection factor. This leads to

$$c = [2e^{ikx}/(\varphi_k(x) - i\varphi_k'(x)/k)]_{x=x_{\max}}. \quad (7)$$

In Fig. 3 we demonstrate the link between HHG and ATI. For three different harmonic orders we plot the recollision

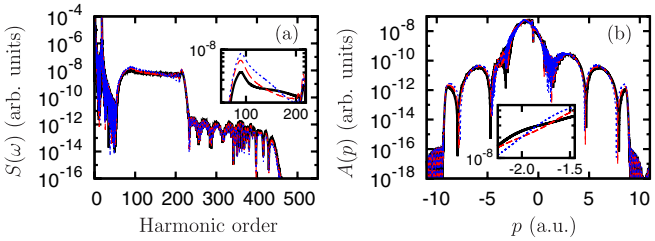

FIG. 2 (color online). (a) HHG spectra for 1D H_2^+ at $R = 2.00$ a.u. (black solid lines), $R = 2.03$ a.u. (red dashed lines), and $R = 2.06$ a.u. (blue dotted lines). (b) ATI momentum distributions. The insets show smoothed details of the spectra.

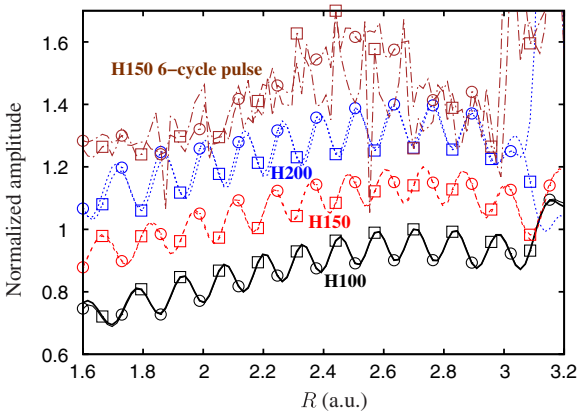

FIG. 3 (color online). HHG recollision amplitude $|a(\omega)|$ (lines with circles) and ATI amplitude $\sqrt{A(p^{(\mathrm{A})}(\omega))}$ (lines with squares) as a function of internuclear distance R for the harmonic orders 100 (black solid lines), 150 (red dashed lines), and 200 (blue dotted lines) and their associated ATI momenta -1.4922 a.u., -1.8301 a.u., and -2.2315 a.u., respectively. The curves were normalized and then shifted vertically pairwise for clarity. Also shown are harmonic 150 and ATI momentum -1.8301 a.u. from a six-cycle trapezoidal pulse with 1-cycle ramps (brown dot-dashed lines), for comparison.

amplitude $|a(\omega)|$ and the ATI amplitude $\sqrt{A(p^{(\mathrm{A})}(\omega))}$ versus R using the pulse of Fig. 1(b). The remarkable overlap between HHG and ATI confirms the strong link between HHG and ATI indicated by the black solid line in Fig. 1(a). This means that $C(\omega)$ is independent of R [34]. The oscillations in Fig. 3 are caused by excitation to the first excited state before ionization, a process that is sensitive to the excitation energy. We have verified that the excitation energy drops by exactly the laser frequency from one maximum to the next. Thus, the oscillation as a function of R becomes slower as we increase the laser frequency (not shown). The HHG and ATI curves for a six-cycle pulse are less similar to each other and exhibit irregular behavior due to multiple trajectories contributing to the yields.

The link between HHG and ATI gives the experimentalist access to the ratio of the instantaneous ionization rates of different molecules during the high-harmonic generation process, and as such is a useful tool in molecular imaging. In particular, the estimate for the recollision amplitude $a(\omega)$ needed for the tomographic reconstruction of molecular orbitals [3] can be improved by using

$$a(\omega) = a^{(a)}(\omega)\sqrt{A(p^{(\mathrm{A})}(\omega))/A^{(a)}(p^{(\mathrm{A})}(\omega))}. \quad (8)$$

Here the superscript "(a)" denotes quantities belonging to the reference atom in orbital tomography. To demonstrate numerically the possibility of combined HHG-ATI-based molecular imaging, we retrieve the recombination dipole moments for the first excited state of 1D H_2^+ as

$$d_r(\omega) = \alpha(\omega)/a(\omega), \quad (9)$$

with either $a(\omega) = a^{(a)}(\omega)\sqrt{P_{\mathrm{I}}/P_{\mathrm{I}}^{(a)}}$ (HHG-based imaging, improved by the total ionization yield P_{I}), or with Eq. (8) (HHG-ATI-based imaging). We use the parameters $R = 2$, $Z = 1.3$ a.u., and the laser pulse from Fig. 1(b). The harmonic orders 75 to 200 are mapped on ATI momenta ranging from -1.09 to -2.23 a.u. As reference atoms we use 1D softcore models with various nuclear charges $Z^{(a)}$. The results of the simulation are shown in Fig. 4. When the total nuclear charge is identical for the molecule and the reference atom [Fig. 4(b)], the molecular transition moment is accurately retrieved when only HHG from the molecule and atom is available [35], thereby also confirming the quantitative rescattering theory [14]. However, when the nuclear charge does not match [Figs. 4(a) and 4(c)], the propagation step differs and errors arise in the retrieved transition moment. These errors largely disappear by incorporating the information from the ATI electrons in the retrieval, demonstrating the potential of Eq. (8) for orbital tomography and molecular imaging in general. In experiment, the HHG-to-ATI link may suffer from intensity averaging, but the detrimental effect

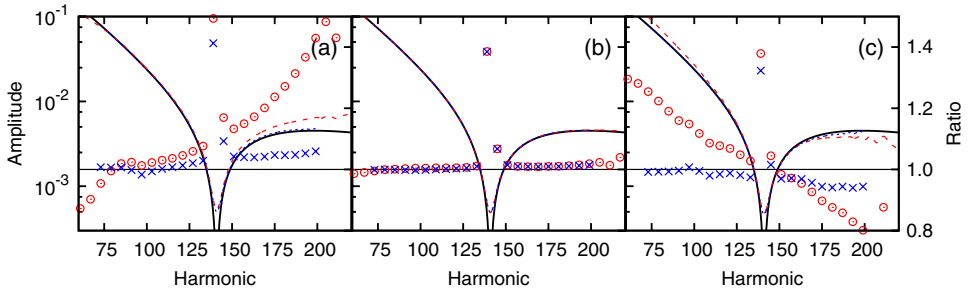

FIG. 4 (color online). Exact recombination transition moment $|d_r(\omega)|$ for the first excited state of 1D H_2^+ (black solid lines), recovered transition moment using HHG-based imaging (red dashed lines) and recovered transition moment using HHG-ATI-based imaging (blue dotted lines) on a logarithmic scale. Also shown is the amplitude ratio of the recovered to the exact transition moments on a linear scale using HHG-based imaging (red circles) and using HHG-ATI-based imaging (blue crosses). Reference atoms with (a) $Z^{(a)} = 1.4$ a.u., (b) $Z^{(a)} = 2.6$ a.u., and (c) $Z^{(a)} = 4$ a.u. are used. The shallowing of the minima comes from diffusing the HHG and ATI spectra with Gaussians with $1/e$ widths of $\Delta\omega = 6\omega_{\mathrm{L}}$ a.u. and $\Delta p = 2\sqrt{0.2\omega_{\mathrm{L}}}$ a.u., respectively.

is reduced by excluding the very low HHG frequencies and ATI momenta.

In summary, we have (i) used the strong-field approximation to design laser pulses for which a one-to-one link between HHG frequencies and ATI momenta holds, (ii) proved this link by numerical solution of the TDSE, (iii) developed a molecular-imaging method utilizing the combined information from HHG and ATI, facilitating highly accurate retrieval of molecular transition moments. Because only the electrons emitted along the polarization axis are needed, the dimensionality should have minor influence on these conclusions, but eventually this will have to be confirmed by full 3D calculations. We expect that future molecular-imaging experiments with aligned molecules will strongly benefit from the present idea by including the orientation dependence of the ATI momentum distributions in the retrieval of molecular properties.

The authors thank Ciprian C. Chirilă for discussions on the saddle-point expression for HHG and the Deutsche Forschungsgemeinschaft for funding the Centre for Quantum Engineering and Space-Time Research (QUEST). We acknowledge the support from the European Marie Curie Initial Training Network Grant No. CA-ITN-214962-FASTQUAST.

[1] M. Ferray, A. L'Huillier, X. F. Li, L. A. Lompre, G. Mainfray, and C. Manus, J. Phys. B **21**, L31 (1988).
[2] M. Lein, N. Hay, R. Velotta, J. P. Marangos, and P. L. Knight, Phys. Rev. A **66**, 023805 (2002).
[3] J. Itatani, J. Levesque, D. Zeidler, H. Niikura, H. Pépin, J. C. Kieffer, P. B. Corkum, and D. M. Villeneuve, Nature (London) **432**, 867 (2004).
[4] T. Kanai, S. Minemoto, and H. Sakai, Nature (London) **435**, 470 (2005).
[5] C. Vozzi, F. Calegari, E. Benedetti, J.-P. Caumes, G. Sansone, S. Stagira, M. Nisoli, R. Torres, E. Heesel, N. Kajumba, J. P. Marangos, C. Altucci, and R. Velotta, Phys. Rev. Lett. **95**, 153902 (2005).
[6] W. Boutu, S. Haessler, H. Merdji, P. Breger, G. Waters, M. Stankiewicz, L. J. Frasinski, R. Taïeb, J. Caillat, A. Maquet, P. Monchicourt, B. Carré, and P. Salières, Nature Phys. **4**, 545 (2008).
[7] B. K. McFarland, J. P. Farrell, P. H. Bucksbaum, and M. Gühr, Science **322**, 1232 (2008).
[8] O. Smirnova, Y. Mairesse, S. Patchkovskii, N. Dudovich, D. Villeneuve, P. Corkum, and M. Y. Ivanov, Nature (London) **460**, 972 (2009).
[9] S. Haessler, J. Caillat, W. Boutu, C. Giovanetti-Teixeira, T. Ruchon, T. Auguste, Z. Diveki, P. Breger, A. Maquet, B. Carré, R. Taïeb, and P. Salières, Nature Phys. **6**, 200 (2010).
[10] C. Vozzi, M. Negro, F. Calegari, G. Sansone, M. Nisoli, S. De Silvestri, and S. Stagira, Nature Phys. **7**, 822 (2011).
[11] H. J. Wörner, J. B. Bertrand, D. V. Kartashov, P. B. Corkum, and D. M. Villeneuve, Nature (London) **466**, 604 (2010).
[12] P. B. Corkum, Phys. Rev. Lett. **71**, 1994 (1993).
[13] E. V. van der Zwan, C. C. Chirilă, and M. Lein, Phys. Rev. A **78**, 033410 (2008).
[14] C. D. Lin, A.-T. Le, Z. Chen, T. Morishita, and R. Lucchese, J. Phys. B **43**, 122001 (2010).
[15] A. D. Shiner, B. E. Schmidt, C. Trallero-Herrero, H. J. Wörner, S. Patchkovskii, P. B. Corkum, J.-C. Kieffer, F. Légaré, and D. M. Villeneuve, Nature Phys. **7**, 464 (2011).
[16] G. Lagmago Kamta and A. D. Bandrauk, Phys. Rev. A **74**, 033415 (2006).
[17] M. Meckel, D. Comtois, D. Zeidler, A. Staudte, D. Pavičić, H. C. Bandulet, H. Pépin, J. C. Kieffer, R. Dörner, D. M. Villeneuve, and P. B. Corkum, Science **320**, 1478 (2008).
[18] M. Lewenstein, P. Balcou, M. Y. Ivanov, A. L'Huillier, and P. B. Corkum, Phys. Rev. A **49**, 2117 (1994).
[19] F. Lindner, M. G. Schätzel, H. Walther, A. Baltuška, E. Goulielmakis, F. Krausz, D. B. Milošević, D. Bauer, W. Becker, and G. G. Paulus, Phys. Rev. Lett. **95**, 040401 (2005).
[20] E. S. Toma, P. Antoine, A. de Bohan, and H. G. Muller, J. Phys. B **32**, 5843 (1999).
[21] M. Y. Kuchiev and V. N. Ostrovsky, J. Phys. B **32**, L189 (1999).
[22] M. Y. Kuchiev and V. N. Ostrovsky, J. Phys. B **34**, 405 (2001).
[23] A.-T. Le, R. R. Lucchese, S. Tonzani, T. Morishita, and C. D. Lin, Phys. Rev. A **80**, 013401 (2009).
[24] C. C. Chirilă and M. Lein, Phys. Rev. A **77**, 043403 (2008).
[25] E. V. van der Zwan and M. Lein, J. Phys. B **41**, 074009 (2008).
[26] M. Y. Ivanov, T. Brabec, and N. Burnett, Phys. Rev. A **54**, 742 (1996).
[27] D. B. Milošević, G. G. Paulus, and W. Becker, Phys. Rev. Lett. **89**, 153001 (2002).
[28] D. B. Milošević, G. G. Paulus, and W. Becker, Laser Phys. **13**, 948 (2003) [http://www.maik.ru/full/lasphys/03/7/lasphys7_03p948full.pdf].
[29] D. B. Milošević, G. G. Paulus, D. Bauer, and W. Becker, J. Phys. B **39**, R203 (2006).
[30] E. V. van der Zwan, Ph.D. thesis, Institut für Physik, University of Kassel, Germany [http://nbn-resolving.de/urn:nbn:de:hebis:34-2011031136492, 2010].
[31] M. D. Feit, J. A. Fleck, Jr., and A. Steiger, J. Comput. Phys. **47**, 412 (1982).
[32] R. Kosloff and H. Tal-Ezer, Chem. Phys. Lett. **127**, 223 (1986).
[33] J. M. Blatt, J. Comput. Phys. **1**, 382 (1967).
[34] See Supplemental Material at http://link.aps.org/supplemental/10.1103/PhysRevLett.108.043004 for more information on the function $C(\omega)$.
[35] D. Zeidler, A. B. Bardon, A. Staudte, D. M. Villeneuve, R. Dörner, and P. B. Corkum, J. Phys. B **39**, L159 (2006).